INITIAL RESULTS FROM THE ISEE-1 AND -2 PLASMA WAVE INVESTIGATION

D. A. GURNETT and R. R. ANDERSON

Department of Physics and Astronomy, The University of Iowa, Iowa City, Iowa 52242, U.S.A.

F. L. SCARF and R. W. FREDRICKS

TRW Defense and Space Systems Group, One Space Park, Redondo Beach, Calif. 90278, U.S.A.

E. J. SMITH

Jet Propulsion Laboratory, 4800 Oak Grove Drive, Pasadena, Calif. 91103, U.S.A.

Abstract. In this paper we present an initial survey of results from the plasma wave experiments on the ISEE-1 and -2 spacecraft which are in nearly identical orbits passing through the Earth's magnetosphere at radial distances out to about $22.5R_e$. Essentially every crossing of the Earth's bow shock can be associated with an intense burst of electrostatic and whistler-mode turbulence at the shock, with substantial wave intensities in both the upstream and downstream regions. Usually the electric and magnetic field spectrum at the shock are quite similar for both spacecraft, although small differences in the detailed structure are sometimes apparent upstream and downstream of the shock, probably due to changes in the motion of the shock or propagation effects. Upstream of the shock emissions are often observed at both the fundamental, f_p^-, and second harmonic, $2f_p^-$, of the electron plasma frequency. In the magnetosphere high resolution spectrograms of the electric field show an extremely complex distribution of plasma and radio emissions, with numerous resonance and cutoff effects. Electron density profiles can be obtained from emissions near the local electron plasma frequency. Comparisons of high resolution spectrograms of whistler-mode emissions such as chorus detected by the two spacecraft usually show a good overall similarity but marked differences in detailed structure on time scales less than one minute. Other types of locally generated waves, such as the $(n+\frac{1}{2})f_g^-$ electron cyclotron waves, show a better correspondence between the two spacecraft. High resolution spectrograms of kilometric radio emissions are also presented which show an extremely complex frequency-time structure with many closely spaced narrow-band emissions.

1. Introduction

In this paper we present a survey of the initial results from the plasma wave investigation on the ISEE-1 and -2 spacecraft, which were launched simultaneously by the same rocket on October 22, 1977. These two spacecraft, which are known as the mother and daughter, are in nearly identical eccentric earth orbits with apogee geocentric radial distances of about $22.5R_e$. Because of the closely matched orbits these two spacecraft provide a unique new capability to resolve spatial and temporal variations in the magnetosphere and solar wind. The separation distance can be controlled by a thruster on ISEE-2 to meet various scientific objectives throughout the mission. For a complete description of the International Sun-Earth Explorer (ISEE) program and the instrumentation on ISEE-1 and -2, see Ogilvie *et al.* (1977).

The plasma wave instruments on ISEE-1 and -2 are designed to provide measurements of the electric and magnetic field of plasma waves over the

Space Science Reviews **23** (1979) 103–122. 0038-6308/79/0231-0103 $03.00.

frequency range from about 5 Hz to 300 kHz. This frequency range includes most of the important characteristic frequencies of the plasma encountered in the magnetosphere and solar wind by these spacecraft. The experimental approach used in the design of these instruments is to provide very complete measurements of plasma wave characteristics (simultaneous electric and magnetic field amplitudes, wave normal and Poynting flux determinations, and high resolution frequency-time spectrograms) on the mother spacecraft (ISEE-1) and somewhat simpler measurements (selected to provide basic space-time correlations) on the daughter spacecraft (ISEE-2). Since the detailed description of the experiment is somewhat involved, the reader is referred to Gurnett *et al.* (1978) for a complete description of the instrumentation. Basically the mother instrument consists of four main elements, (1) a 24-channel high time resolution spectrum analyzer, (2) a narrow-band sweep frequency receiver, (3) a wave normal and Poynting flux analyzer, and (4) a wide-band receiver. These elements can be connected in various combinations to the six plasma wave antennas on ISEE-1, which consist of three electric dipole antennas with tip-to-tip lengths of 215 m, 73.5 m, and 0.61 m, and a set of triaxial search coil antennas. The daughter instrument consists of two main elements, (1) a 16-channel high time resolution spectrum analyzer, and (2) a wide-band receiver, both with bandwidths and characteristics matched to the corresponding elements on the mother spacecraft. The ISEE-2 plasma wave antennas consist of two electric dipole antennas, with tip-to-tip lengths of 30 m and 0.61 m and one search coil magnetic antenna. Signals from only one of these antennas can be analyzed at a time.

The primary purpose of this report is to present some of the initial results from this investigation and to comment on the overall performance and operation of the instrument. Since only a few months of data are currently available for analysis, the depth of analysis and comparisons with other instruments are necessarily limited. However, as will be seen, the plasma wave instruments on the ISEE-1 and -2 spacecraft are providing very exciting new measurements which have the potential of making a significant advance in our understanding of magnetospheric plasma waves.

2. A Survey of Some Representative Passes

To illustrate the variety of observations which are being obtained we have selected several representative passes for detailed analysis and comment. The first example selected is the inbound pass on day 309, November 5, 1977. This pass enters the magnetosphere on the day side of the Earth, near local noon, and has been selected because of the well defined bow shock and magnetopause crossings which occurred on this day. The electric field intensities from the high time resolution spectrum analyzers on ISEE-1 and -2 during this day are shown in Figures 1 and 2, respectively. The field strengths are on a logarithmic scale with a 100 dB dynamic range from the baseline of one channel to the baseline of the

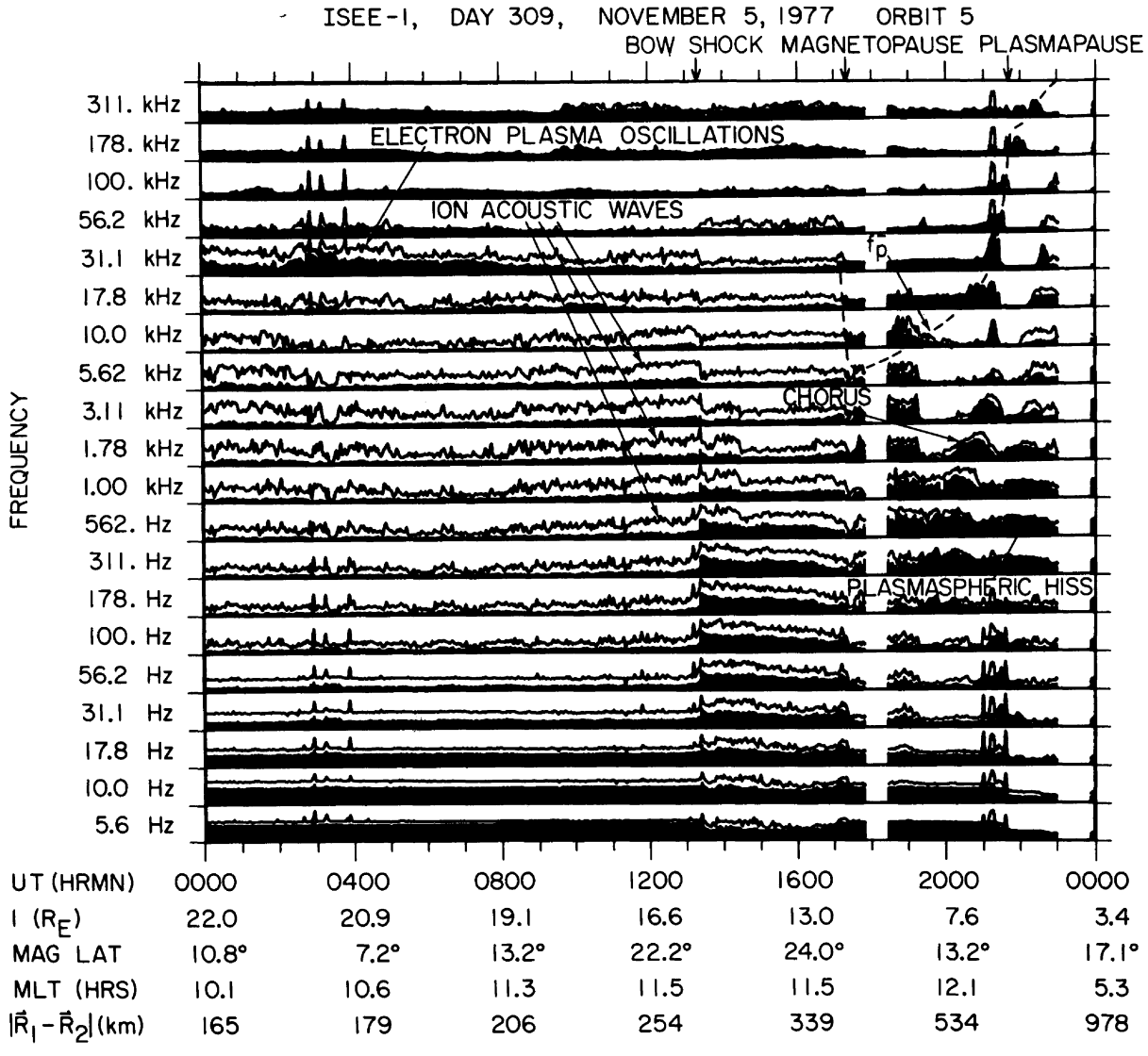

Fig. 1. The electric field amplitudes from the 24-channel high time resolution spectrum analyzer on ISEE-1 for the inbound magnetospheric pass on day 309, 1977. The dynamic range for each channel is 100 dB. The solid line gives the peak field strength and the solid black area indicates the average field strength.

next higher channel. This range extends from about 0.1 μV m^{-1} to 10.0 mV m^{-1} for the ISEE-1 data and from about 0.15 μV m^{-1} to 15.0 mV m^{-1} for the ISEE-2 data. The solid lines gives the maximum electric field strength and the solid black area gives the average electric field strength. The bow shock crossing is evident from the very abrupt increase in the electric field intensities at about 13:23 UT. The magnetopause crossing on this pass occurs at about 17:10 to 17:20 UT, and the plasmapause crossing occurs at about 21:35 UT.

On the coarse time scale shown in Figures 1 and 2 the electric field intensity variations show a remarkably close correspondence between ISEE-1 and -2 in all regions of the magnetosphere and solar wind. In the solar wind the most prominent types of waves are the electron plasma oscillations in the 31.1 kHz channel and the ion-acoustic waves in the channels from about 100 Hz to 10 kHz. Previous studies have shown that the electron plasma oscillations are produced by

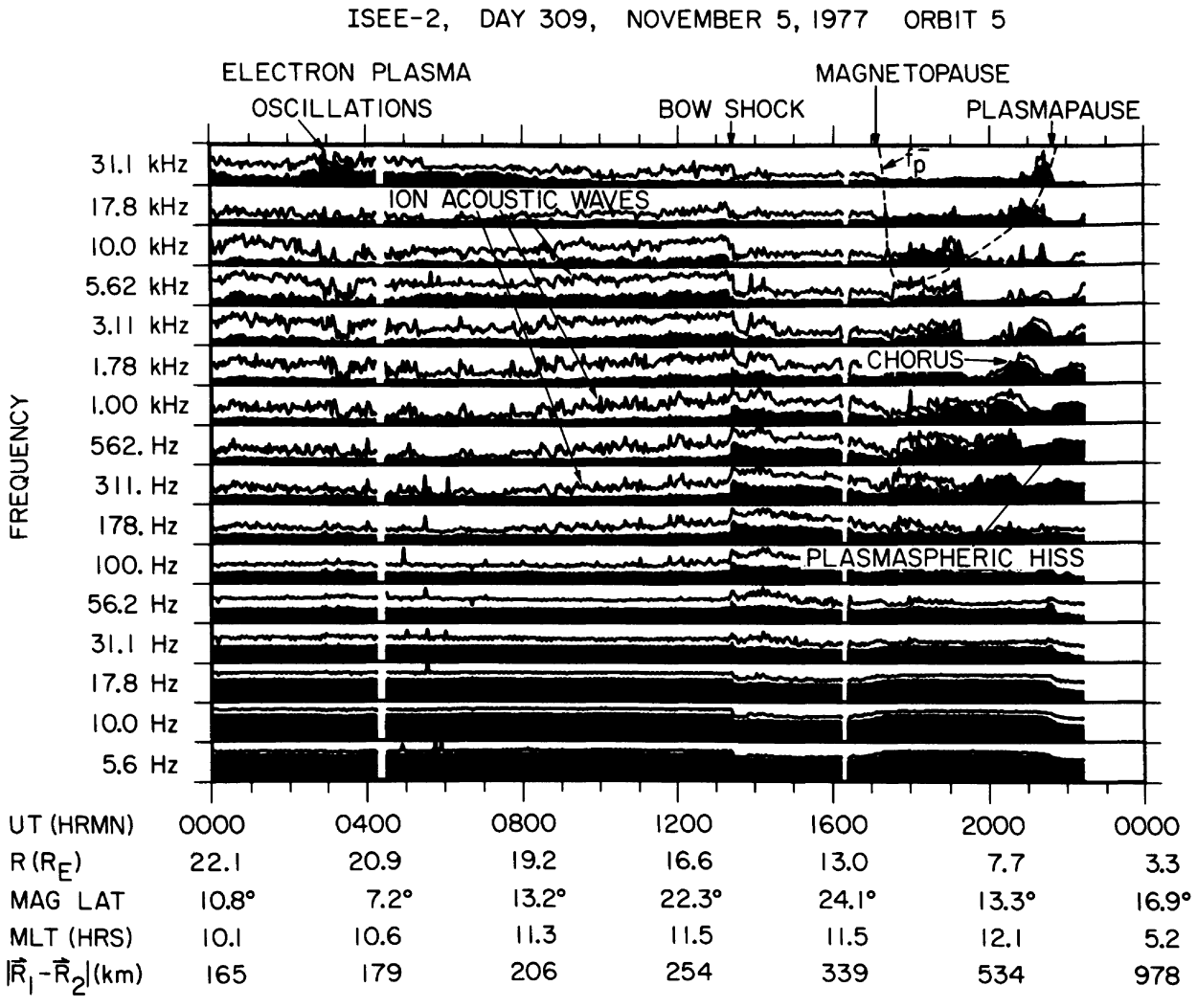

Fig. 2. The electric field amplitudes from the 16-channel spectrum analyzer on ISEE-2 for the same pass as in Figure 1. On this coarse time scale the electric field intensities on ISEE-1 and -2 show a very close correspondence.

electrons streaming into the solar wind from the bow shock (Scarf *et al.*, 1971) and that the ion-acoustic waves, based on the mode identification by Gurnett and Frank (1978), are produced by protons streaming into the solar wind from the bow shock (Scarf *et al.*, 1970). Comparisons of the electric field strength obtained by the different length antennas on the two spacecraft provide an interesting check on the wavelength of these two types of waves. Detailed comparisons show that the electric field strengths of the plasma oscillations, computed using an effective length equal to one-half of the tip-to-tip length of the antennas, are in very close agreement ($\pm 10\%$) between the two spacecraft. This close agreement confirms that the wavelength of the electron plasma oscillations is substantially longer than the length of the longest antenna (215 m). This conclusion is in agreement with the results of Gurnett and Frank (1975), who estimated that the wavelength of the upstream electron plasma oscillations is of the order of several kilometers. In contrast to the electron plasma oscillations, the computed electric

field strengths of the upstream ion-acoustic waves near the frequency of maximum intensity (3.11 and 5.62 kHz) are about a factor of 5 to 15 larger for the shorter (30 m) ISEE-2 antenna compared to the longer (215 m) ISEE-1 antenna. This difference in the computed electric field strengths indicates that these waves have wavelengths substantially shorter than the length of the longest antenna ($\lambda \leqslant$ 215 m). This conclusion confirms the earlier results of Gurnett and Frank (1978), who showed that these waves have relatively short wavelength, near $2\pi\lambda_D$ where λ_D is the Debye length, as would be expected for the ion-acoustic mode. For such short wavelengths the frequency is mainly determined by the Doppler shift.

At the bow shock substantial differences in the electric field intensities are evident when the data are examined on a fine time scale. A detailed high time resolution comparison of the electric field intensities near the shock crossing is shown in Figure 3, together with the magnetic field strength obtained from the UCLA magnetometer (data provided by C. Russell). As can be seen in Figure 3 the difference in the times of the shock crossing is readily apparent between the two spacecraft. These time delays have been analyzed by Russell *et al.* (1978) to provide estimates of the shock velocity. Comparisons of the electric field intensity variations through the shock show the same general overall characteristic for both spacecraft, with a broad peak lasting several tens of seconds near the ramp in the magnetic field, and significant differences in the fine structure. The width of the transition region appears to be somewhat larger for ISEE-1 than for ISEE-2.

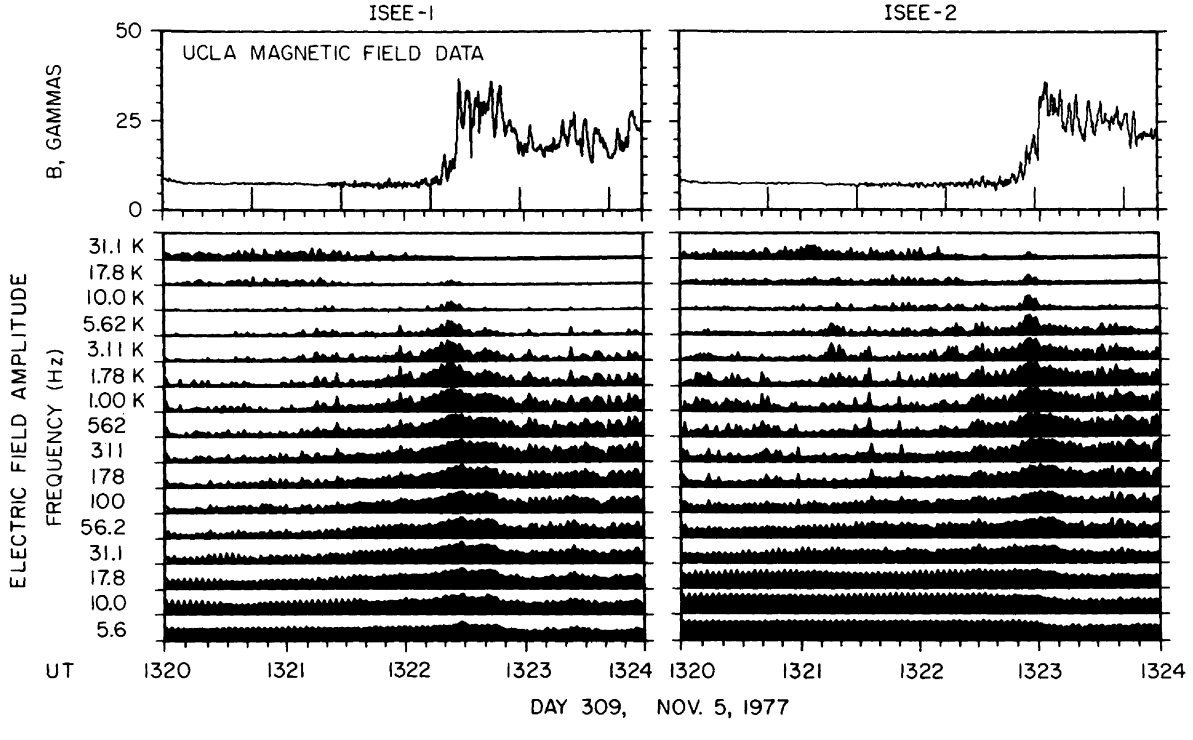

Fig. 3. High time resolution details of the electric field intensity variations at the bow shock crossing on day 309, 1977. The difference in the shock crossing times due to the separation between the two spacecraft is clearly evident. Although the overall structure of the electric field turbulence is similar at the two spacecraft, significant differences can be seen in the fine time scale structure.

Differences in the detailed temporal structure of the electron plasma oscillations are also evident upstream of the shock. Although differences in detail can be seen upstream and downstream of the shock, the electric field spectrums averaged over 16 s around the times of peak intensity are quite similar for the two spacecraft, as shown in Figure 4. Both spectrums show a very broad nearly flat plateau extending up to about 3 kHz and are very similar to the shock spectrums previously published by Rodriguez and Gurnett (1975) from the IMP-6 spacecraft. Above 3 kHz the ISEE-1 and -2 spectrums deviate considerably, with the largest field strengths being detected by ISEE-2. This deviation at high

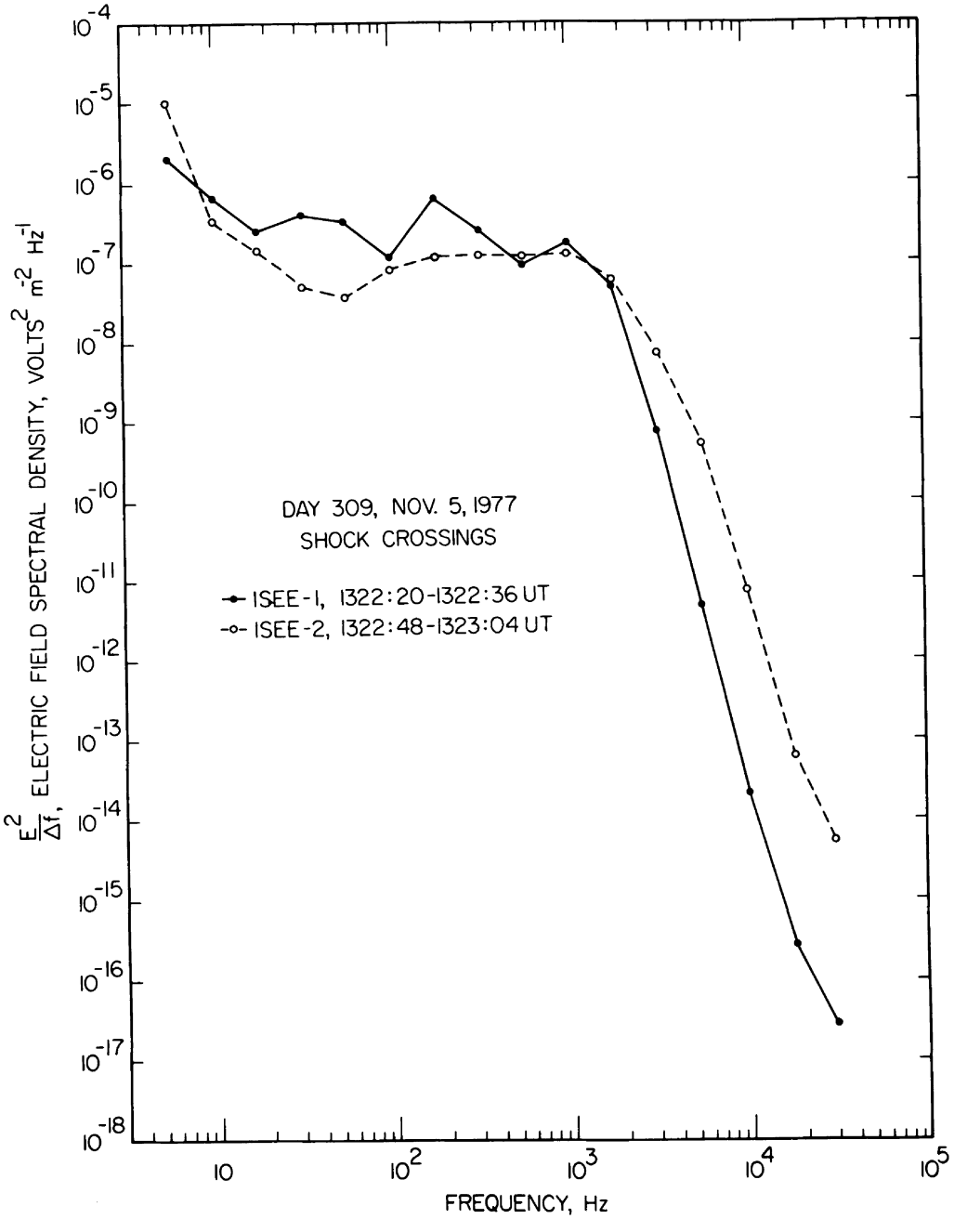

Fig. 4. The electric field spectrums at the times of peak intensity for the two shock crossings shown in Figure 3. The two spectrums are very similar except at high frequencies.

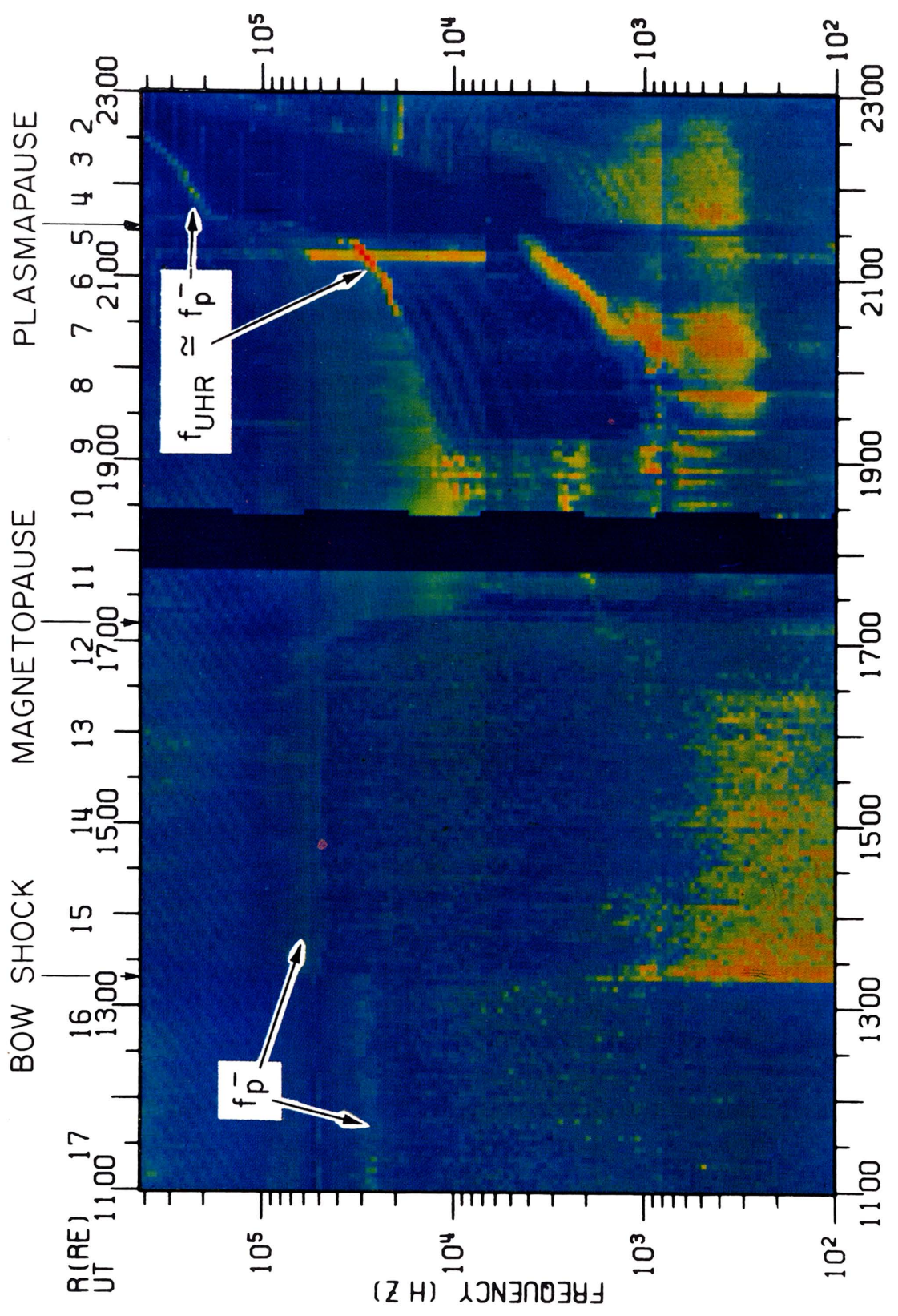

Fig. 5. The narrow-band sweep frequency receiver data for the same inbound pass shown in Figure 1. This receiver provides essentially constant fractional frequency resolution over a very wide frequency range, from 100 Hz to 400 kHz, and dynamic range, 100 dB. Very accurate electron density contours can be obtained from the emissions at the electron plasma frequency and upper hybrid resonance frequency and from the continuum radiation cutoff at the electron plasma frequency.

frequencies could be an indication that wavelengths shorter than 215 m are being detected at frequencies above 3 kHz.

In the magnetosheath behind the shock a broad spectrum of electric field turbulence is evident extending from below 5.62 Hz up to about 100 kHz. This electric field turbulence has been previously described by Rodriguez (1978) and is believed to be due to either ion-acoustic waves or Buneman mode waves (Buneman, 1958) at low frequencies, <10 kHz, and electron plasma oscillations at high frequencies, ~ 56.2 kHz. A slight enhancement in the electric field intensities can be seen at low frequencies, <100 Hz, near the magnetopause boundary, possibly indicating the generation of plasma wave turbulence in association with this boundary.

Inside of the magnetosphere the plasma wave spectrum is much more complicated than in the solar wind and magnetosheath. The analysis of the plasma wave spectrums in this region is greatly aided by the data from the narrow-band sweep frequency receiver shown in Figure 5. This receiver provides an essentially constant resolution logarithmic frequency scan, with $\Delta f/f \simeq 6.5\%$, from 100 Hz to 400 kHz. The bow shock, magnetopause and plasmapause can be readily identified, as indicated at the top of the spectrogram. One of the most striking features of this spectrogram is the extent to which the electron plasma frequency, f_p^-, can be identified through essentially the entire orbit. In the solar wind and magnetosheath the electric field emissions near the plasma frequency are caused by electron plasma oscillations, of the type previously discussed. Inside of the magnetosphere the electron plasma oscillations are no longer present. However, the electron plasma frequency can still be identified from the low frequency cutoff of the continuum radiation trapped in the low density cavity between the magnetopause and plasmapause (Gurnett and Shaw, 1973) and from narrow-band emissions at the upper hybrid resonance frequency, f_{UHR}, inside of the plasmasphere (Mosier *et al.*, 1973). For the high density conditions inside of the plasmapause, $f_g^- \ll f_p^-$, the upper hybrid resonance is approximately equal to the electron plasma frequency ($f_{UHR} = \sqrt{f_p^{-2} + f_g^{-2}}$, where f_g^- is the electron gyrofrequency). This ability to identify the electron plasma frequency from the plasma wave data provides a valuable method of obtaining very accurate sheath independent measurements of the plasma density.

Many other characteristic emission frequencies and cutoff effects can also be identified in Figure 5. Beyond the plasmapause, from about 19:15 to 21:35 UT, several very weak, few $\mu V\,m^{-1}$, narrow-band emissions can be identified near half-integral harmonics of the electron cyclotron frequency, $(n+\frac{1}{2})f_g^-$. These weak emissions correspond to the diffuse $(n+\frac{1}{2})f_g^-$ electrostatic bands described by Shaw and Gurnett (1975). At larger radial distances, from about 17:30 to 19:15 UT, the $(n+\frac{1}{2})f_g^-$ electrostatic emissions at $(\frac{3}{2})f_g^-$ and $(\frac{5}{2})f_g^-$ become much more intense ranging from several hundred $\mu V\,m^{-1}$ to about one $mV\,m^{-1}$. These more intense $(n+\frac{1}{2})f_g^-$ electrostatic emissions are believed to correspond to the $(\frac{3}{2})f_g^-$ and $(\frac{5}{2})f_g^-$ electrostatic waves first reported by Kennel *et al.* (1970) and

discussed by Young *et al.* (1973), Ashour-Abdalla and Kennel (1978) and others. At about 21:05 to 21:10 UT a very intense narrow-band emission occurs near the upper hybrid resonance frequency, $f_{UHR} \simeq 30$ kHz. This emission is so strong that it saturates the ISEE-1 narrow-band receiver, causing the dark vertical band in Figure 5. The field strength of this emission can be determined from the multi-channel spectrum analyzer, which is not saturated, and is about 7.73 mV m^{-1}. Intense narrow-band emissions of this type are frequently observed near the upper hybrid resonance outside of the plasmapause (see Figure 13 of Gurnett, 1975) and are thought to be related to the generation of the continuum radiation which occurs in this frequency range. These narrow-band emissions near the upper hybrid resonance are one of the most intense electrostatic waves encountered anywhere in the magnetosphere. Other effects which can be identified in Figure 5 include (1) signals from ground VLF transmitters, at about 20 kHz inside of the plasmasphere from 22:10 to 23:00 UT, (2) an upper frequency cutoff for the whistler-mode noise inside the plasmasphere at about $0.6f_g^-$, due to cyclotron damping, (3) plasmaspheric hiss, from about 300 Hz to 3 kHz inside of the plasmasphere, (4) chorus from about 1 to 3 kHz outside of the plasmasphere and (5) several periods of intense auroral kilometric radiation at frequencies above 100 kHz.

To further illustrate the complex structure of the magnetospheric electric field emissions Figures 6 and 7 show two more spectrograms from the narrow-band sweep frequency receiver. These spectrograms show the inbound portions of two successive passes through the magnetosphere approximately two days apart, on December 28 and December 30, 1977. Essentially all of the features remarked on in Figure 5 are again evident on these passes. One noteworthy effect is the abrupt decrease in the **upper** hybrid resonance frequency, hence plasma density, at about 11:55 UT on December 28 and an almost identical decrease on the same L-shell two days later, at about 21:15 UT on December 30. Evidently this depression in the plasma density represents a relatively long-lived feature of the plasmaspheric density distribution which took several days to decay. Another noteworthy effect is the series of type III solar radio events evident in Figure 6 at frequencies above about 100 kHz. These events can be clearly identified by their characteristic frequency-time dispersion, decreasing in frequency with increasing time. One of these events, from about 11:20 to 12:00 UT, shows a sharp low frequency cutoff in almost exact correspondence with the narrow-band **upper** hybrid resonance emission. This propagation cutoff provides a particularly convincing identification of the local electron plasma frequency, which for the conditions present ($f_g^- \ll f_p^-$) is essentially identical to the **upper** hybrid resonance frequency.

3. High Resolution Comparisons of Chorus and $(n+\frac{1}{2})f_g^-$ Noise Bands

For purposes of making very high time resolution comparisons both the ISEE-1 and ISEE-2 plasma wave instruments contain identical wide-band receivers which

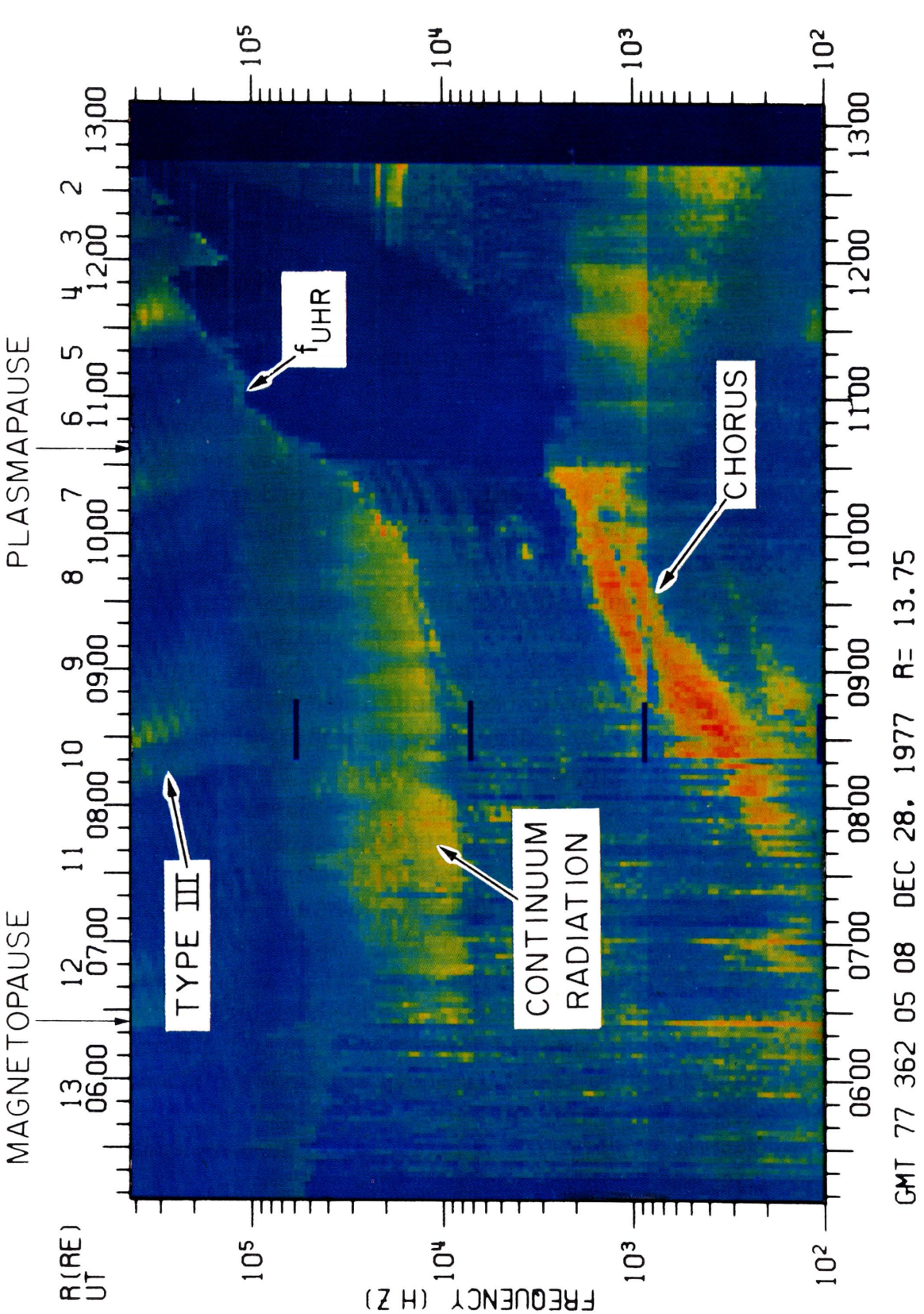

Fig. 6. Another spectrogram from the narrow-band sweep frequency receiver on ISEE-1 illustrating the repeated occurrence of many of the same plasma wave emissions shown in Figure 5.

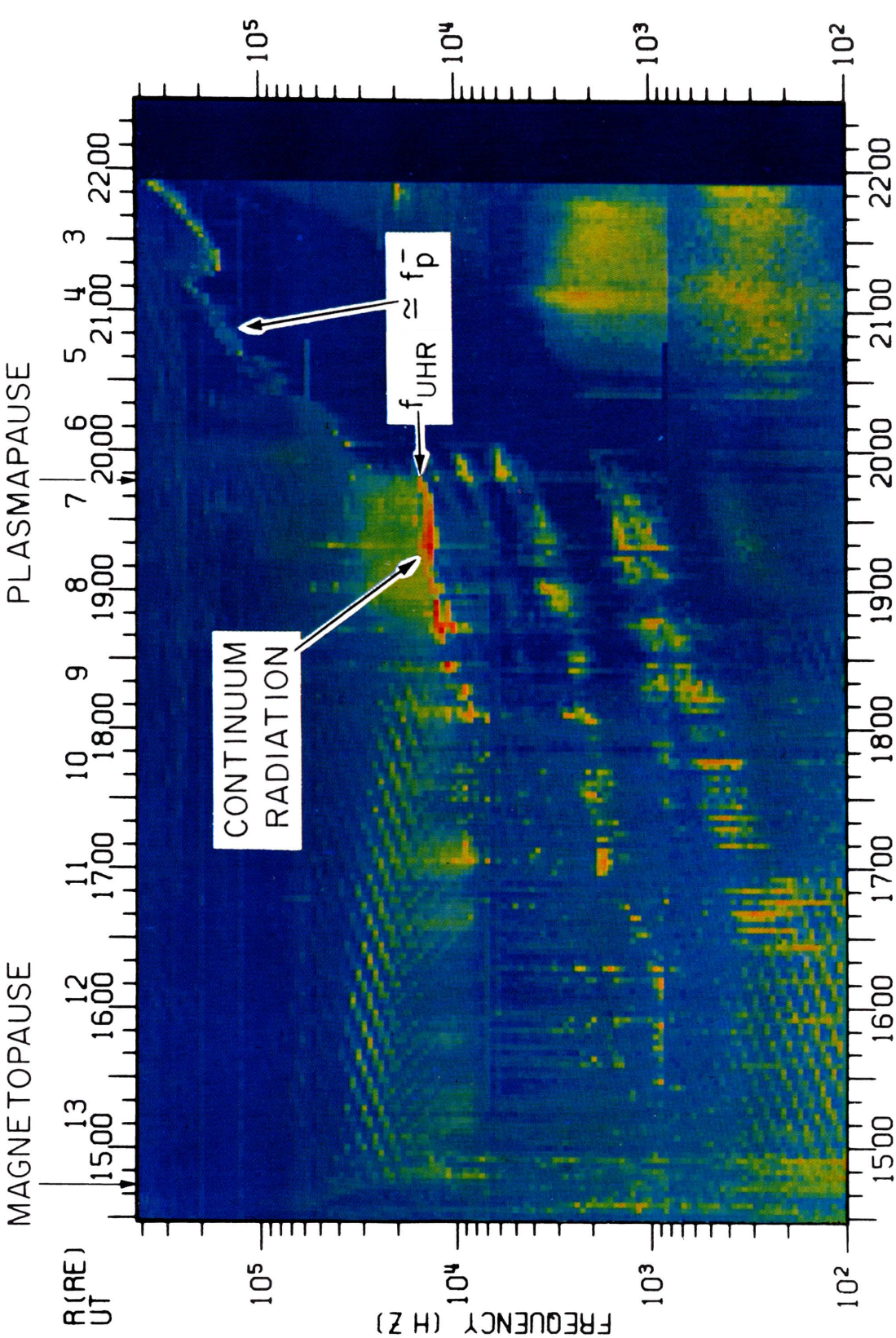

Fig. 7. The sweep frequency receiver spectrogram for the next pass following pass in Figure 6. Of special interest is the small depression in the electron density within the plasmasphere which apparently persists for the two-day interval between these passes.

can be used to transmit electric and magnetic field waveforms to the ground for detailed spectrum analysis. This capability permits measurements to the limit of the uncertainty principle, $\Delta f \Delta t \sim 1$, so that very small propagation delays can be detected and analyzed. A typical example of the wide-band electric field data from ISEE-1 and -2 is shown in Figure 8. This illustration shows frequency-time spectrograms of whistler-mode chorus emissions selected from the inbound pass on day 309, 1977, which was discussed earlier. Although the spectrums at the two spacecraft show good overall similarity on a time scale of a few minutes or more, it is extremely difficult to identify corresponding bursts of noise on time scales of a few seconds or less. During this period the spacecraft are separated by distances on the order of 450 km. For this separation distance the time difference for the two spacecraft to pass through the same region of space is about 160 s, and the whistler-mode time delay is on the order of a few tenths of a second. Detailed comparisons by overlaying the two spectrograms show that it is impossible to arrive at a simple time delay, either due to the spacecraft transit time or due to propagation delays, which can bring the two spectrums into alignment. Thus, for separation distances of 400 km the electric field spectrums do not correlate well on small time scales of a few minutes or less. Chorus spectrograms examined on other orbits show a similar effect. Although a more involved cross-correlation analysis may later reveal a better correlation, simple comparisons of the chorus

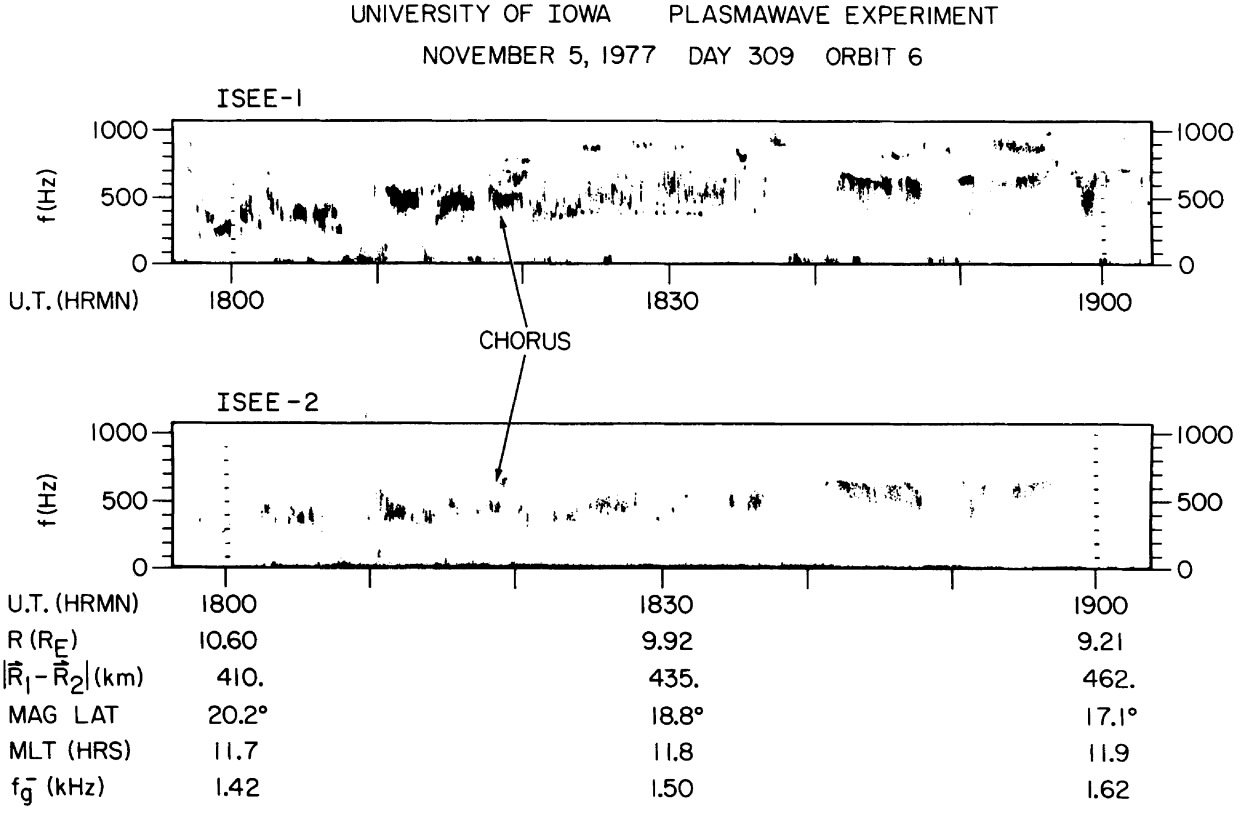

Fig. 8. High time resolution spectrograms of chorus emissions from the wideband receivers on ISEE-1 and -2. Although the chorus emissions are seen to occur in the same general frequency range at the two spacecraft, very marked differences are evident in the detailed temporal structure which cannot be accounted for by simple time delays.

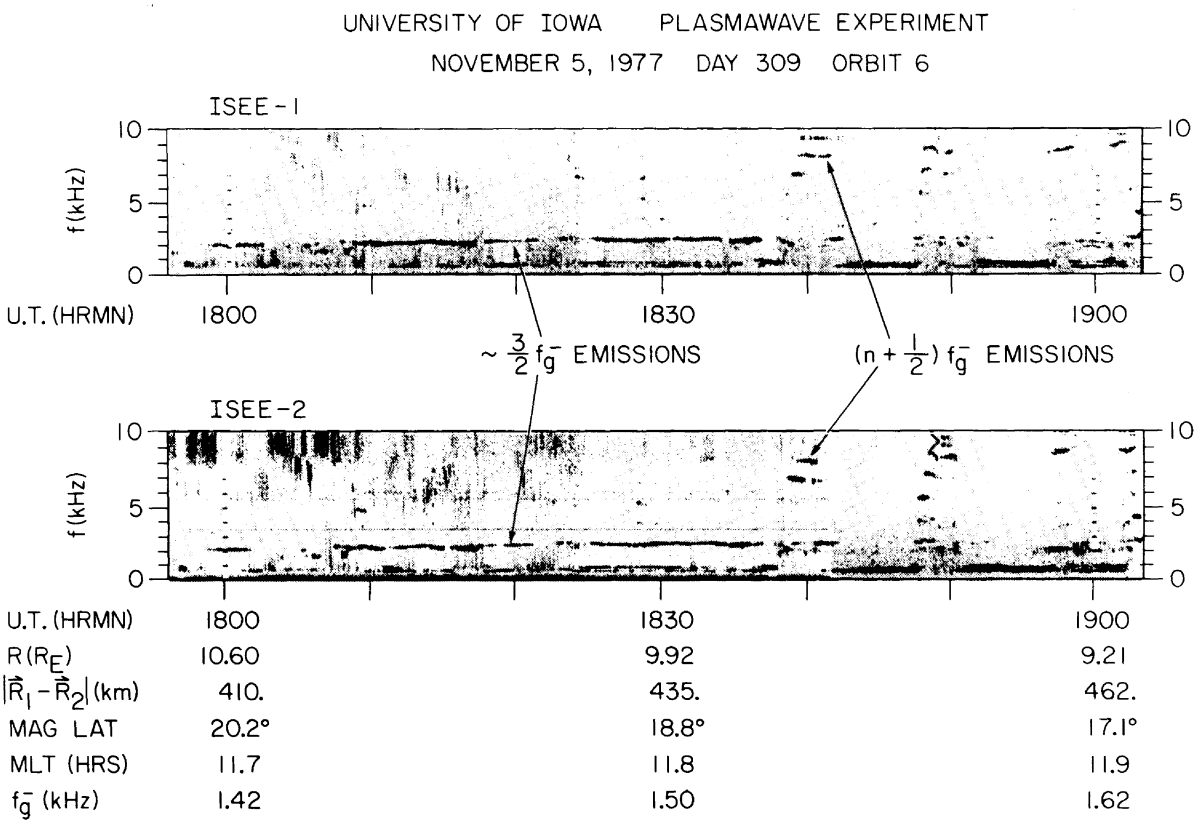

Fig. 9. High time resolution spectrums of $(n+\frac{1}{2})f_g^-$ electrostatic emissions detected by ISEE-1 and -2. In this case a reasonably good correspondence in the overall structure of the emissions can be obtained if the spectrums are shifted to account for the transit time of spacecraft, which in this case is about 160 s. Significant differences in the fine structure are, however, still evident.

spectrograms indicate that the size of the wave packets responsible for the chorus emissions is small compared to a few hundred km and that considerable small scale spatial structure exists in the chorus emissions.

Similar high resolution frequency-time spectrograms of the $(\frac{3}{2})f_g^-$ electrostatic emissions observed on day 309, 1977, are shown in Figure 9 from about 17:30 to 19:15 UT. These spectrograms again show that on a time scale of a few minutes or longer the 'same' emission can be identified on both spacecraft, but that on shorter time scales the detailed correlation tends to be rather poor. In this case careful comparisons show that the correlation between certain features, such as the gaps in the $(\frac{3}{2})f_g^-$ band and the bursts of high order $(n+\frac{1}{2})f_g^-$ emissions, is improved if the ISEE-2 spectrogram is shifted to the left by about 160 s to account for the spacecraft transit time. Many small scale differences, however, still exist. Another example of the $(n+\frac{1}{2})f_g^-$ electrostatic emissions from day 326, November 22, 1977, is shown in Figure 10. In this case the detailed correspondence in the frequency variations caused by changes in the magnetic field strength is well correlated between the two spacecraft, and can be brought into good correspondence by shifting the ISEE-2 spectrogram to the left by about 160 s to account for the spacecraft transit time. Again, even though the large scale features can be brought into good correspondence, many of the features on time scales less

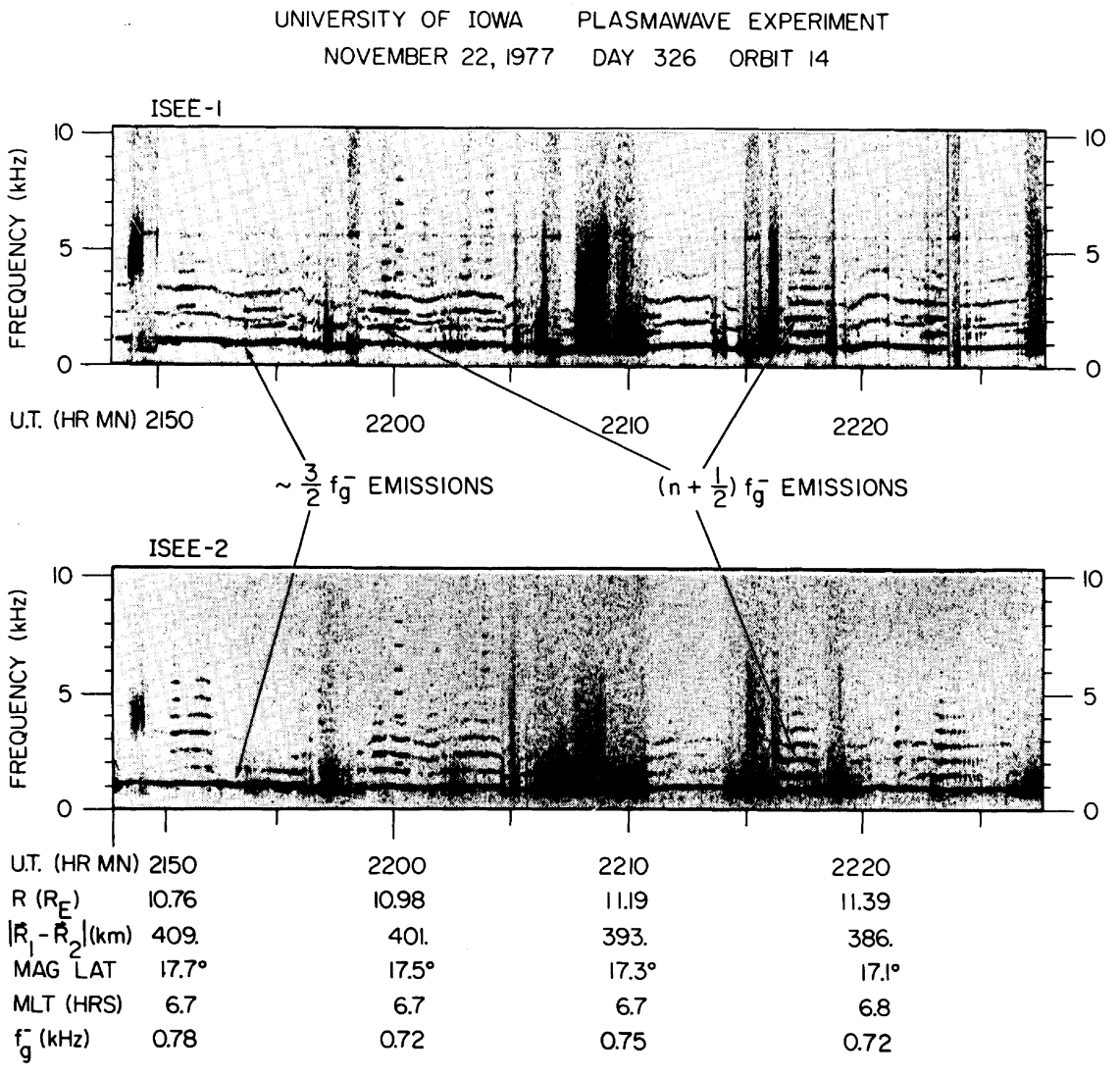

Fig. 10. Another example of the $(n+\frac{1}{2})f_g^-$ electrostatic noise bands illustrating the good overall correspondence in the structure and frequency variations observed by the two spacecraft as well as the differences in the fine structure.

than one minute are not well correlated. The overall conclusion from these comparisons is that the $(n+\frac{1}{2})f_g^-$ electrostatic emissions show a better correlation between the two spacecraft than the chorus emissions. However, neither type of emission shows a good correspondence on small time scales, less than one minute. This result is not considered unexpected since the electrostatic $(n+\frac{1}{2})f_g^-$ emissions have much lower phase velocities than the electromagnetic chorus emissions and should display a spatial structure characteristic of a localized non-propagating wave.

4. High Resolution Spectrums of Auroral Kilometric Radiation

In order to provide high resolution frequency-time spectrograms of high frequency radio emissions from the earth and other solar system radio sources the ISEE-1 and -2 wide-band receivers can be tuned, using frequency conversion techniques, to a variety of frequencies extending up to 2.0 MHz. This frequency

conversion mode of operation has produced some particularly interesting results for periods when intense bursts of auroral kilometric radiation were being detected by ISEE-1 and -2. This radiation is generated at relatively low altitudes in the auroral regions and is closely correlated with the occurrence of discrete auroral arcs (see for example, Gurnett, 1974; Kurth *et al.*, 1975; Alexander and Kaiser, 1976; and Green *et al.*, 1977).

An example of a period when intense auroral kilometric radiation is being detected by ISEE-1 and -2 is shown in Figure 11. A long period of intense kilometric radiation activity can be seen in the 100, 178, and 311 kKz channels, extending from about 04:30 UT to the end of the day. During this period the wide-band receiver was operated for a short period, from 04:45 to 06:40 UT, in the 500 kHz frequency conversion mode. In this mode waveform signals in the frequency band from 500 to 540 kHz are converted to 0 to 40 kHz and transmitted back to the ground. The electric field intensity in the 500 to 540 kHz frequency band is shown in the top channel of Figure 11. As can be seen the

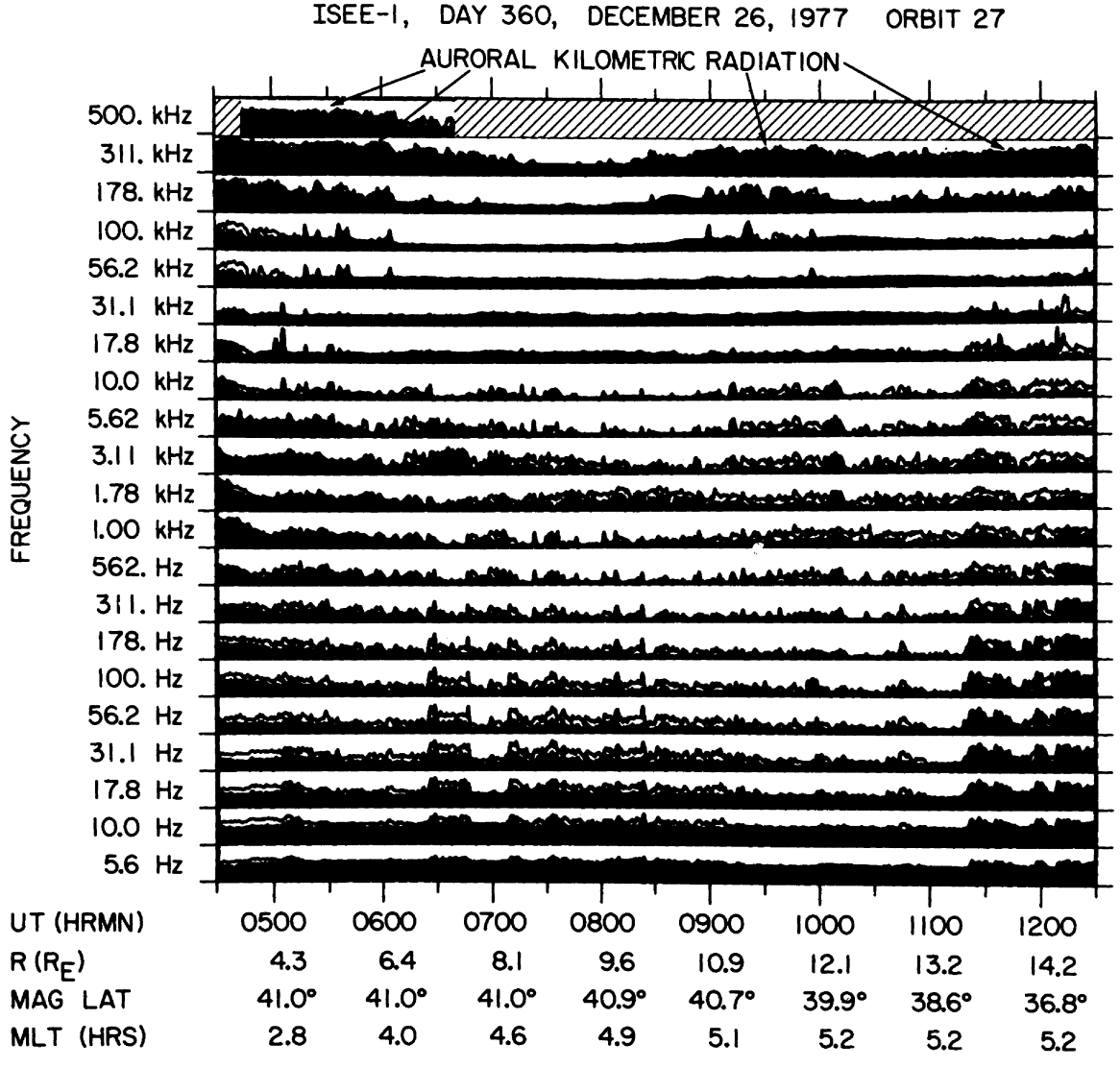

Fig. 11. An example of a period when intense kilometric radio emissions are being detected by ISEE-1 in the frequency range from 100 to 500 kHz.

auroral kilometric radiation spectrum at this time extends from about 100 kHz to well above 500 kHz.

The high resolution frequency-time spectrograms of the auroral kilometric radiation detected during this time in the narrow frequency band from 500 to 540 kHz are shown in Figure 12. As can be seen the spectrum has an astonishing amount of fine structure, consisting of many narrow-band emissions with rapidly

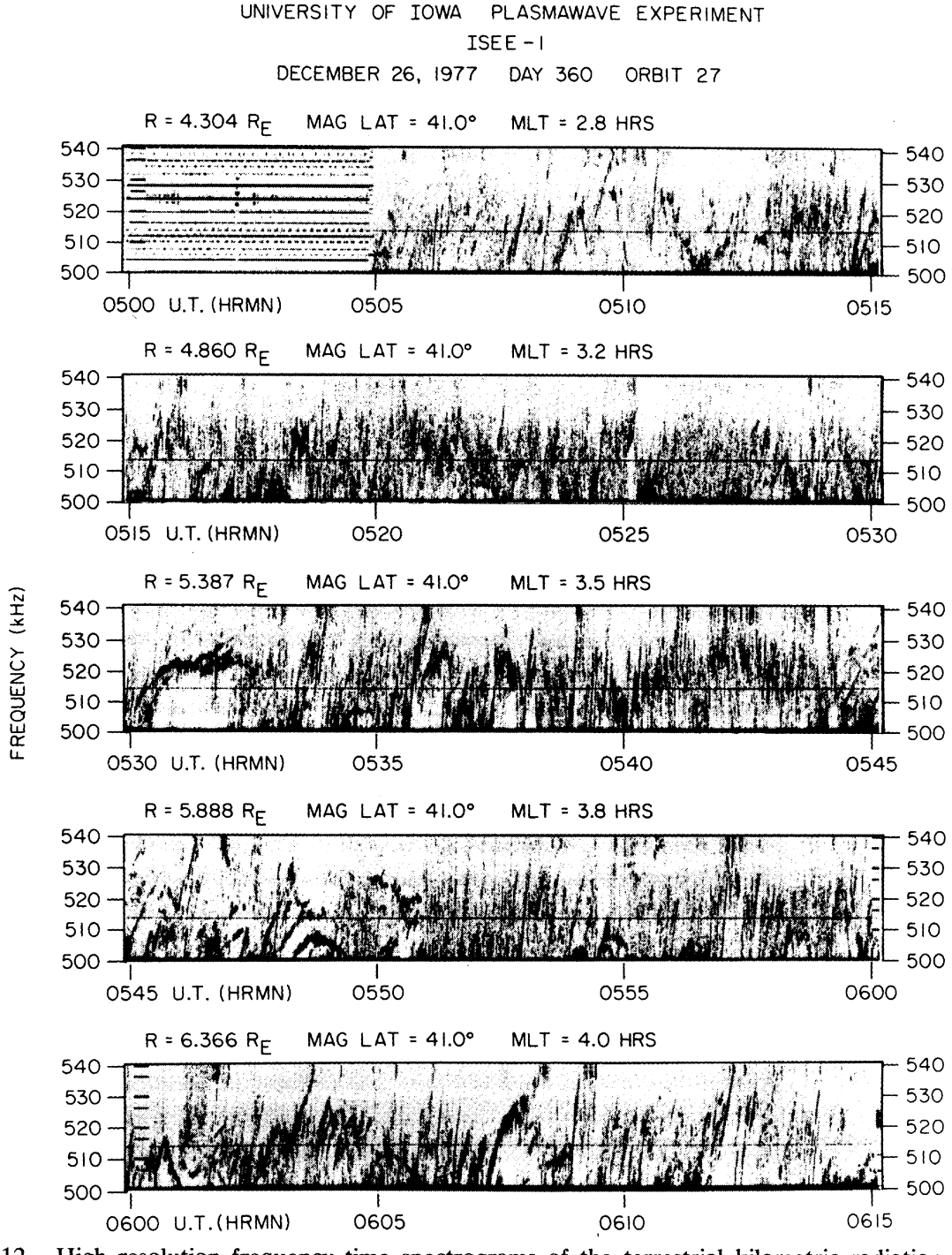

Fig. 12. High resolution frequency time spectrograms of the terrestrial kilometric radiation from the wideband receiver on ISEE-1 for the same event shown in Figure 11. These spectrograms, which cover the narrow frequency range from 500 to 540 kHz, show that the kilometric radiation has a great deal of fine structure, often consisting of narrowband emissions increasing in frequency with increasing time.

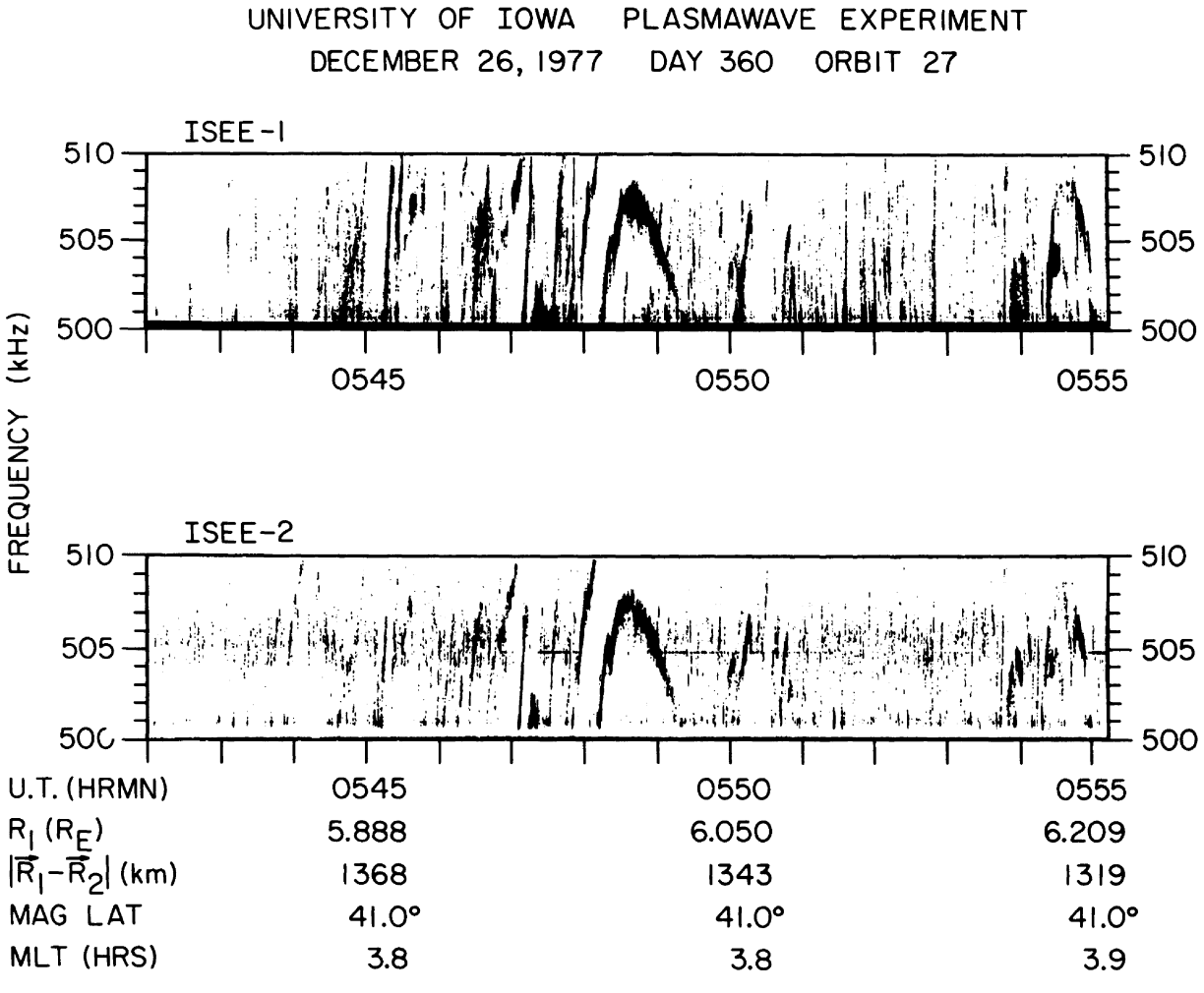

Fig. 13. A comparison of the wideband spectrograms of the kilometric radiation detected simultaneously by ISEE-1 and -2. Because of the small separation distance the time delay between the two spacecraft, ~4 ms, is too small to be resolved on these spectrograms. Later, more detailed analyses using techniques of long baseline interferometry will give very accurate information on the source position and motion from data such as these.

varying center frequencies. In many cases the frequency of these emissions appears to be increasing with increasing time. A few cases are evident for which the frequency rises, reaches a maximum, and then starts to decrease, for example at about 05:44 UT, giving an inverted U-shaped appearance on the frequency-time spectrogram. Comparisons of ISEE-1 and -2 show almost identical spectrums for this radiation, as would be expected since the radiation is propagating at frequencies well above the local electron plasma frequencies, where local plasma effects should not be important. Corresponding ISEE-1 and -2 spectrograms in the frequency range from 500 to 510 kHz are shown in Figure 13. Since the radiation is propagating at the speed of light, the time delay expected between the two spectrums is quite small, only about 4.5 ms. Because the time delay is so small we have not yet attempted to measure it, since a fairly elaborate cross-correlation analysis will be required to provide good accuracy. However, such measurements are possible and can be used to provide information on the source position and motion using standard techniques of long baseline interferometry. Appropriate

reference signals are transmitted to the ground from each spacecraft so that phase interferometry measurements can be made between the two spacecraft.

The complex frequency-time structure of the auroral kilometric radiation is a new characteristic which has never been previously observed. Although unexpected, the occurrences of bursts with rapidly drifting center frequencies is not unusual in other astrophysical radio sources, and is a common feature of solar radio bursts (Kundu, 1965) and Jovian decametric radio emissions (Warwick, 1967). Usually such features are interpreted as being due to the motion of the emitting particles, or some other disturbance, through a plasma which has a spatial gradient in the characteristic emission frequencies, as for example in type III and type IV solar radio bursts. If we adopt this explanation for the frequency drift of the auroral kilometric radiation, an estimate can be made for the velocity of the source. From Figure 12 the drift rate of a typical burst can be estimated to be about $df/dt = 2.0\ \text{kHz s}^{-1}$. This value is representative, for example, of the bursts from about 05:51 to 05:54 UT. To translate this drift rate into a source velocity some assumptions must be made about the characteristic frequencies of the plasma in the source region. For the terrestrial kilometric radiation it is widely believed that the radiation is generated at relatively low altitudes of about 1 to $2R_e$ along the auroral field lines. Although it is not known whether the emission frequency is more closely associated with the electron gyrofrequency or the electron plasma frequency, at these altitudes the radial gradients of these two characteristic frequencies are roughly comparable. Using the ionospheric model given by Gurnett (1974), the radial gradients in the electron gyrofrequency and plasma frequency are approximately, $df/dR = 0.2\ \text{kHz km}^{-1}$. For the observed drift rates the corresponding velocity of the source is $dR/dt = (dR/df)(df/dt) = 10\ \text{km s}^{-1}$. Since the drift rate is positive and the characteristic frequencies of the plasma increase with decreasing radial distance the source motion is toward the Earth. Exceptions to this motion do of course occur, for example in the case of the inverted-U shaped bursts. However, most of the bursts in Figure 12 can be accounted for by a source moving down the auroral field lines at a velocity of about $10\ \text{km s}^{-1}$.

Having estimated the approximate velocity of the source attention can now be given to the question of whether this source motion corresponds to an actual motion of the emitting particles, or to some other type of disturbance propagating down the auroral field lines. If the frequency drift is caused by the motion of the emitting particles then the corresponding energies for electrons and protons would be 2.8×10^{-4} and 0.5 eV. These energies are so small compared to the thermal energies of the auroral plasma that it is not reasonable to attribute the frequency drift directly to the motion of the particles emitting the radiation. Some type of propagating disturbance is needed to explain the observed frequency drift. One interesting possibility is that the source motion may be related to the transient motion of an electrostatic shock or double layer along the auroral field line since the inferred source velocity of $\sim 10\ \text{km s}^{-1}$ is comparable to the

ion-acoustic speed in the auroral ionosphere. This mechanism would be somewhat analogous to the generation of a drifting type IV solar radio burst by a shock propagating through the solar corona.

5. Conclusion

In this paper we have presented a survey of the initial results from the ISEE-1 and -2 plasma wave investigation. These results demonstrate the very high quality data which are being obtained from these instruments and illustrate the wide range of magnetospheric plasma physics problems which can be attacked using these spacecraft. The plasma wave spectrum comparisons between the two spacecraft illustrate the great advantages of using two spacecraft in similar orbits to unravel the complex spatial and temporal variations which occur in the magnetosphere. Clearly, the complexities are such that a great deal of additional work is needed to fully understand the spatial and temporal structure of magnetospheric plasma waves and their relationship to the magnetospheric charged particle distribution. These studies will be our primary objective during the next several years.

Acknowledgements

We are very thankful to Dan Odem and his team at the University of Iowa, consisting of Roger D. Anderson, Bill Walker, Keith Baker, and Don Kirchner, who carried out the design and construction of these large and complex instruments. Special thanks are also given to Robert Shaw of the University of Iowa who helped direct this project while the Principal Investigator (D. Gurnett) was on sabbatical leave. We are also indebted to Allan Frandsen of JPL and Paul Virobik of TRW for their contribution to the design and construction of the search coil and short electric antenna. We are also very grateful for the fine support and cooperation of the many members of the ISEE Project at GSFC and ESTEC who made this mission a success. Special thanks is also given to C. Russell of UCLA for providing the magnetic field data and to P. Jepsen of JPL and W. Kurth of the University of Iowa for their efforts in producing the color spectrograms.

This research was supported by NASA under Contract NAS5-20093 from Goddard Space Flight Center and Grant NGL-16-001-043.

References

Alexander, J. K. and Kaiser, M. L.: 1976, 'Terrestrial Kilometric Radiation, 1. Spatial Structure Studies', *J. Geophys. Res.* **81,** 5948.

Ashour-Abdalla, M. and Kennel, C. F.: 1978, 'Nonconvective and Convective Electron Cyclotron Harmonic Instabilities', *J. Geophys. Res.* **83,** 1531.

Buneman, O.: 1958, 'Instability, Turbulence and Conductivity in a Current Carrying Plasma', *Phys. Rev. Letters* **1,** 8.

Green, J. L., Gurnett, D. A., and Shawhan, S. D.: 1977, 'The Angular Distribution of Auroral Kilometric Radiation', *J. Geophys. Res.* **82,** 1825.

Gurnett, D. A.: 1974, 'The Earth as a Radio Source: Terrestrial Kilometric Radiation', *J. Geophys. Res.* **79,** 4227.

Gurnett, D. A.: 1975, 'The Earth as a Radio Source: the Non-Thermal Continuum', *J. Geophys. Res.* **80,** 2751.

Gurnett, D. A. and Frank, L. A.: 1975, 'Electron Plasma Oscillations Associated with Type III Radio Emissions and Solar Electrons', *Solar Phys.* **45,** 477.

Gurnett, D. A. and Frank, L. A.: 1978, 'Ion-Acoustic Waves in the Solar Wind', *J. Geophys. Res.* **83,** 58.

Gurnett, D. A., Scarf, F. L., Fredricks, R. W., and Smith, E. J.: 1978, 'The ISEE-1 and -2 Plasma Wave Investigation', *IEEE Trans. Geosci. Electr.* **GE-16,** 225.

Gurnett, D. A. and Shaw, R. R.: 1973, 'Electromagnetic Radiation Trapped in the Magnetosphere Above the Plasma Frequency', *J. Geophys. Res.* **78,** 8136.

Kennel, C. F., Scarf, F. L., Fredricks, R. W., McGehee, J. H., and Coroniti, F. V.: 1970, 'VLF Electric Field Observations in the Magnetosphere', *J. Geophys. Res.* **75,** 6136.

Kundu, M. R.: 1965, *Solar Radio Astronomy*, Interscience Publishers, New York.

Kurth, W. S., Baumback, M. M., and Gurnett, D. A.: 1975, 'Direction-Finding Measurements of Auroral Kilometric Radiation', *J. Geophys. Res.* **80,** 2764.

Mosier, S. R., Kaiser, M. L., and Brown, L. W.: 1973, 'Observations of Noise Bands Associated with the Upper Hybrid Resonance by the IMP-6 Radio Astronomy Experiment', *J. Geophys. Res.* **78,** 1673.

Ogilvie, K. W., von Rosenvinge, T., and Durney, A. C.: 1977, 'International Sun-Earth Explorer: a Three-Spacecraft Mission', *Science* **198,** 131.

Rodriguez, P.: 1978, 'Magnetosheath Electrostatic Turbulence', *J. Geophys. Res.*, accepted for publication.

Rodriguez, P. and Gurnett, D. A.: 1975, 'Electrostatic and Electromagnetic Turbulence Associated with the Earth's Bow Shock', *J. Geophys. Res.* **80,** 19.

Russell, C. T. and Greenstadt, E. W.: 1979, 'Initial ISEE Magnetometer Results: Shock Observations', *Space Sci. Rev.* **23,** 3.

Scarf, F. L., Fredricks, R. W., Frank, L. A., Russell, C. T., Coleman, P. J., Jr., and Neugebauer, M.: 1970, 'Direction Correlations of Large-Amplitude Waves with Suprathermal Protons in the Upstream Solar Wind', *J. Geophys. Res.* **75,** 7316.

Scarf, F. L., Fredricks, R. W., Frank, L. A., and Neugebauer, M.: 1971, 'Non-Thermal Electrons and High-Frequency Waves in the Upstream Solar Wind, 1. Observations', *J. Geophys. Res.* **76,** 5162.

Shaw, R. R. and Gurnett, D. A.: 1975, 'Electrostatic Noise Bands Associated with the Electron Gyrofrequency and Plasma Frequency in the Outer Magnetosphere', *J. Geophys. Res.* **80,** 4259.

Warwick, J. W.: 1967, 'Radiophysics of Jupiter', *Space Sci. Rev.* **6,** 841.

Young, T. S. T., Callen, J. D., and McCune, J. E.: 1973, 'High-Frequency Electrostatic Waves in the Magnetosphere', *J. Geophys. Res.* **78,** 1082.